



Article

# Effects of Nitrogen Modification of Porous PVD–MoS<sub>2</sub> Coatings on the Tribological Behavior under Rolling–Sliding Conditions in Vacuum

Armin Seynstahl <sup>1,\*</sup>, Markus Polzer <sup>2</sup>, Marcel Bartz <sup>2</sup>, Sandro Wartzack <sup>2</sup> and Stephan Tremmel <sup>1</sup><sup>1</sup> Engineering Design and CAD, Universität Bayreuth, Universitätsstr. 30, 95447 Bayreuth, Germany; stephan.tremmel@uni-bayreuth.de<sup>2</sup> Engineering Design, Friedrich-Alexander-Universität Erlangen-Nürnberg (FAU), Martensstr. 9, 91058 Erlangen, Germany; polzer@mfk.fau.de (M.P.); bartz@mfk.fau.de (M.B.); wartzack@mfk.fau.de (S.W.)

\* Correspondence: armin.seynstahl@uni-bayreuth.de

**Abstract:** In order to improve the tribological performance of PVD–MoS<sub>2</sub> coatings, which are frequently used as a solid lubricant for operating in challenging environments, e.g., in a vacuum, they can be modified with nitrogen. This work evaluates the tribological behavior and a possible compaction occurring during the initial tribological load in the rolling contact for pure and nitrogen-modified PVD–MoS<sub>2</sub> coatings in a vacuum. Short-running tests (1000 cycles) of coated steel discs paired with uncoated steel discs made from 100Cr6 (1.3505, AISI 52100) were conducted on a two-disc tribometer. The slide-to-roll ratio of 10.5% was kept constant, while the load was varied in two steps from 1.1 GPa to 1.6 GPa. Subsequently, a comparison was made between the worn and the pristine coatings by means of nanoindentation and an optical analysis of the wear track. The formation of a load-bearing solid lubrication was achieved for both MoS<sub>2</sub>-variants. The main differences affected the material transfer and wear mechanisms. The worn coatings reached a similar wear coefficient of  $4 \times 10^{-6} \text{ mm}^3 \text{N}^{-1} \text{m}^{-1}$  and a possible compaction of the coatings was found, indicated through an increased indentation hardness (for MoS<sub>2</sub> 1158% and MoS<sub>2</sub>:N 96% at a 1.1 GPa load). The assumed tribological mechanism changed with nitrogen modification, but scales with increasing load. The nitrogen-modified MoS<sub>2</sub> coating showed less compaction than pure MoS<sub>2</sub>, while the frictional behavior was improved by a 17% reduction of the coefficient of friction.

**Keywords:** MoS<sub>2</sub>; tribology; vacuum; solid lubrication; transfer layer; two-disc

**Citation:** Seynstahl, A.; Polzer, M.; Bartz, M.; Wartzack, S.; Tremmel, S. Effects of Nitrogen Modification of Porous PVD–MoS<sub>2</sub> Coatings on the Tribological Behavior under Rolling–Sliding Conditions in Vacuum. *Lubricants* **2023**, *11*, 335. <https://doi.org/10.3390/lubricants11080335>

Received: 27 June 2023

Revised: 21 July 2023

Accepted: 5 August 2023

Published: 8 August 2023



**Copyright:** © 2023 by the authors. Licensee MDPI, Basel, Switzerland. This article is an open access article distributed under the terms and conditions of the Creative Commons Attribution (CC BY) license (<https://creativecommons.org/licenses/by/4.0/>).

## 1. Introduction

The solid lubricant molybdenum disulfide (MoS<sub>2</sub>) is widely employed in challenging environments where conventional oil and grease lubrication are ineffective or undesirable [1,2]. Application proved particularly effective at low temperatures [3,4], high temperatures [5,6], and, especially, under vacuum conditions, for instance, in space applications [7–10]. Therefore, a common technique for applying such coatings is the (reactive) physical vapor deposition (PVD) process. Under vacuum conditions, the layered microstructure [11] of MoS<sub>2</sub> unfolds its full potential due to the easy sliding of the individual MoS<sub>2</sub> lamellae against each other. In combination with the coating transfer to the counterpart and the formation of a tribofilm, this results in a self-lubrication mechanism [12,13]. Conversely, it means excellent tribological behavior, which is reflected in very low coefficients of friction (COFs) [8,14,15] and low wear [16,17]. The preferred layer growth of MoS<sub>2</sub> coatings for tribological applications is the basal orientation, which is characterized by MoS<sub>2</sub> lamellae aligned parallel to the substrate and is associated with good lubrication performance and a prolonged service life [18–22], although, in the case of sputter-deposited coatings, an initial basal orientation may not be achieved, resulting in vertical [23,24] or nanocrystalline [25,26] growth, which, in turn, tends to be accompanied by lower lubrication performance. To

alleviate these structural issues, which may be detrimental to coating performance, MoS<sub>2</sub> coatings were often co-sputtered with metals such as titanium (Ti), chromium (Cr) [27–29], gold (Au) [30,31], or silver (Ag) [32] in the past. Also, the combination with diamond-like carbon (DLC) coatings receives attention in the literature [33,34]. Another approach to increase coating performance is the combination of different coating types, the so-called “chameleon coatings”. This ensures that the best coating works under the particular operating conditions (temperature, relative humidity, and load case) [35,36]. The improvement of the coatings by means of modification with gaseous nitrogen has been given less consideration, and even only in the last few years [37–41]. While the tribological behavior (friction and wear) of MoS<sub>2</sub> coatings in the literature is most often represented by simple model tests, such as pin (ball)-on-disc tests, these studies often refer only to sliding contact conditions. Investigations on nitrogen-modified coatings under rolling conditions are still completely lacking.

For tribological experiments under rolling–sliding conditions, a two-disc tribometer (2DT) can be used for a variety of materials and lubricants [42–45]. The 2DT is applicable for the characterization of tribological systems in a wide range, from pure sliding to various slip conditions to pure rolling. With regard to tooth flanks or rolling bearings, findings from tests in 2DTs are more transferable than those from the ball-on-disc tests usually performed, and allow the possibility of high Hertzian contact stresses. While the investigations mainly focus on the testing of tribologically effective thin coatings or bearing steel under oil lubrication conditions, the two-disc test rig is also a suitable test method for dry lubrication conditions [42–44,46,47].

Hence, the aim of our work presented here is to obtain a more precise understanding of the tribological behavior of sputter-deposited MoS<sub>2</sub>-based coatings in rolling–sliding contact conditions. For this purpose, tribological experiments were carried out on a novel 2DT under vacuum conditions for the first time. Two coatings were investigated: pure MoS<sub>2</sub> and a nitrogen-modified variant, which shall henceforth be referred to as MoS<sub>2</sub>:N. The tribological tests run up to 1000 cycles while the load was varied in two steps, allowing, in particular, a comparison of the running-in behavior. The appearing wear phenomena were evaluated visually, post mortem. To identify tribologically induced changes, nanoindentation measurements were conducted before and after the tribological loading of the coatings.

## 2. Materials and Methods

### 2.1. Specimens, Coatings, and Deposition Process

For tribological experiments, discs (height  $h = 10$  mm; diameter  $d = 45$  mm) made from rolling bearing steel 100Cr6 (1.3505, AISI 52100) were used. Half of the samples were cylindrical, serving as substrates for coating deposition, and half were crowned with a secondary curvature of  $R = 42$  mm, being the counterparts in the two-disc tests. Additionally, for reference measurements, planar specimens were coated on their face side. All specimens were hardened and tempered to provide a hardness of  $62 \pm 1$  HRC. The lateral surface of the discs was fine-polished to a roughness  $R_a < 0.03$   $\mu\text{m}$  (Bestenlehrer GmbH, Herzogenaurach, Germany). Prior to charging the specimens, they were ultrasonically cleaned in acetone and in isopropyl alcohol for 10 min each and blown dry with nitrogen.

The coatings were deposited utilizing an industrial-scale PVD coating unit (TT 300 K4, H-O-T Härte- und Oberflächentechnik GmbH & Co. KG, Nuremberg, Germany). The process used in this study refers to PVD and reactive PVD. Preceding the deposition process, the coating chamber was evacuated to reach an initial pressure of  $2.5 \times 10^{-3}$  Pa and heated to 50 °C for 15 min. Furthermore, the surface of the specimens was plasma-etched and cleaned by argon (Ar+)-ion plasma etching for 15 min, working with an argon (Ar purity 99.999%) gas flow of 500 sccm and a bipolar pulsed bias voltage of -500 V (pulse frequency 40 kHz, reverse recovery time 5  $\mu\text{s}$ ). Subsequently, a sputtering process was carried out for 3 min with closed shutters to remove impurities and the thin oxide layer from the hot-pressed MoS<sub>2</sub> powder targets (purity of 99.5%). The targets were positioned opposite

to each other in the coating chamber and had a dimension of 260 × 163 mm (Sindlhauser GmbH, Kempten, Germany).

For this study, two coatings based on MoS<sub>2</sub> were fabricated by (reactive) PVD through unbalanced magnetron (UBM) sputtering in argon atmosphere. The threefold substrate rotation (rotational speed of 6 rpm) ensured that all specimens were coated homogeneously on all sides. The pure MoS<sub>2</sub> coating was fabricated with a previously thin reactive sputtered adhesive layer. In this case, the adhesion layer was applied by reactive sputtering for 240 s with 20 sccm nitrogen and 240 s with 14 sccm, and, afterwards, the MoS<sub>2</sub> layer was deposited by non-reactive UBM sputtering. For chemically modifying the pure MoS<sub>2</sub> coating, nitrogen (N<sub>2</sub> purity 99.999%) was introduced at 15 sccm throughout the process to ensure that the modification was homogeneously distributed over the entire growth time of the coating. No adhesive layer was applied for this coating. Both coatings were each deposited on four test specimens and compared in two different test settings, respectively. The relevant deposition parameters are listed in Table 1.

**Table 1.** Relevant deposition parameters for the pure and the nitrogen-modified MoS<sub>2</sub> coating.

Deposition Parameters	MoS <sub>2</sub>	MoS <sub>2</sub> :N
Adhesion layer duration in s	480	-
Functional layer duration in s	3600	4200
Sputtering power in kW	2.0	
Bias voltage in V	-100	
Argon gas flow in sccm	120	
Nitrogen gas flow in sccm	-	15
Temperature (chamber) in °C	50	

## 2.2. Coating Characterization

The characterization of the as-deposited coatings is of major interest. Thickness and surface topography are to be documented as references. Coating thickness was measured on the flat specimens by laser scanning microscopy (LSM, VK-X200, Keyence Corp., Osaka, Japan) using the incremental step method. For this purpose, a small area of the substrate surface was masked with Kapton® tape prior to deposition process to create a step jump between the substrate and the coating, from which the coating thickness was averaged by three measurements. Roughness parameters and surface topography were also analyzed optically by LSM.

In order to investigate the differences in the mechanical properties of the coatings, the indentation hardness  $H_{IT}$  and the indentation modulus  $E_{IT}$  were determined on the discs for the pristine coatings via nanoindentation (Picodentor HM500 and WinHCU, Helmut Fischer GmbH, Sindelfingen, Germany) according to Oliver and Pharr [48,49]. A Vickers indenter was used for the measurement with a maximum indentation force of 1.0 mN. The measurements were performed in the enhanced stiffness procedure (ESP) mode, with incremental loading and unloading processes. Using this method, the mechanical properties ( $H_{IT}$ ,  $E_{IT}$ ) can be calculated at any point on the measurement curve in relation to force and depth. Here, the evaluation was carried out at  $5\% \pm 1\%$  of the respective coating thickness in order to minimize the substrate influence and to evaluate below 10% of the coating thickness according to Bückle's rule [50]. Eight indentations were made for each of the four measurements per disc and the arithmetic mean was determined for the indentation hardness  $H_{IT}$  and the indentation modulus  $E_{IT}$ .

Scanning electron microscopy (SEM) was conducted to identify the chemical composition and, thus, the S/Mo-ratio of the coatings via energy dispersive X-ray spectroscopy (EDS) mappings and to verify the formation of a transfer layer on the counterpart after the tribological tests. Therefore, a FEI Helios Nanolab 600i (ThermoFisher Scientific, Waltham, MA, USA) equipped with an Xmax<sup>50</sup> detector (Oxford Instruments, Abingdon, UK) was used.

### 2.3. Tribological Testing

Tribological testing was executed on a two-disc tribometer (2DT, Optimol Instruments Prüftechnik GmbH, Munich, Germany) under vacuum conditions (pressure 0.2 Pa) and at room temperature (RT) with a constant slide-to-roll ratio (SRR); load was varied in two steps. In this study, the coated cylindrical discs were pressed against uncoated crowned discs (Figure 1) to simulate the contact conditions similar to rolling bearings.

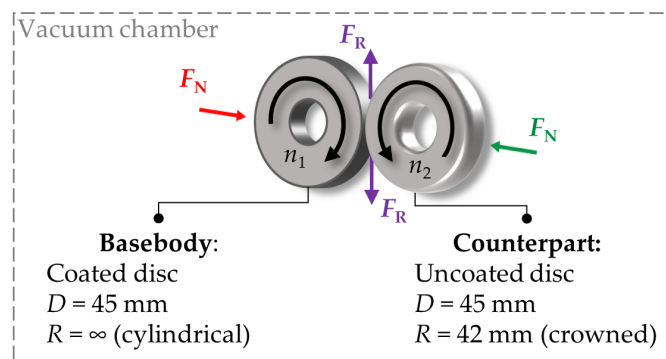


**Figure 1.** Schematic illustration of the 2DT set-up and geometry of the specimens.

The speeds of the discs were chosen to achieve a differential circumferential speed  $\Delta v$  of  $0.1 \text{ ms}^{-1}$  and an SRR of 10.5%. Two series of tests were carried out with normal loads of 265 N and 675 N, respectively, corresponding to initial Hertzian pressures at the contact center of approximately 1.1 GPa and 1.6 GPa. The relevant parameters of the tribological tests are summarized in Table 2.

**Table 2.** Load cases for the tribological testing using the 2DT.

Load Case	1	2
$F_N$ in N	265	675
$p_{\max}$ in GPa	1.1	1.6
$n_1$ in rpm	423	
$n_2$ in rpm	381	
$\Delta v$ in $\text{ms}^{-1}$	0.1	
Cycles $n_{\text{total}}$	1000	
$T$ in $^{\circ}\text{C}$	RT	
Repetitions $n$	2	
SRR in %	10.5	

The rotational speed of the discs and the load were chosen to be comparable as much as possible to previous studies from Seynstahl et al. [22], which were executed on a ball-on-disc tribometer. That means load case 1 aimed to mimic the sliding contact from the ball-on-disc tests by setting the difference in rotational velocities of the two discs to  $0.1 \text{ ms}^{-1}$ , and to adjust the load, resulting in the same maximum Hertzian pressure of 1.1 GPa at the contact center. To evaluate the influence of a higher applied normal force on the tribological behavior, load case 2 with a maximum pressure of 1.6 GPa was employed. By measuring the friction force (data acquisition rate of 50 Hz) in the two-disc tests, the coefficients of friction (COFs) over the running time or revolutions could be determined directly. The revolutions are referred to as cycles hereinafter, following [22]. Since tribological run-in processes and initial compaction of the coating are of primary interest, the tests were limited to 1000 cycles. In addition, the specimens were inspected visually post mortem and ex situ to determine any sign of wear, and the compaction of the coating by comparing initial and residual coating thickness in the wear track and possible transfer layer formation. In order to identify possible compaction of the coatings after wear testing, the indentation hardness  $H_{\text{IT}}$  and the indentation modulus  $E_{\text{IT}}$  were determined accordingly to 2.2 inside the wear track; see Figure 2.

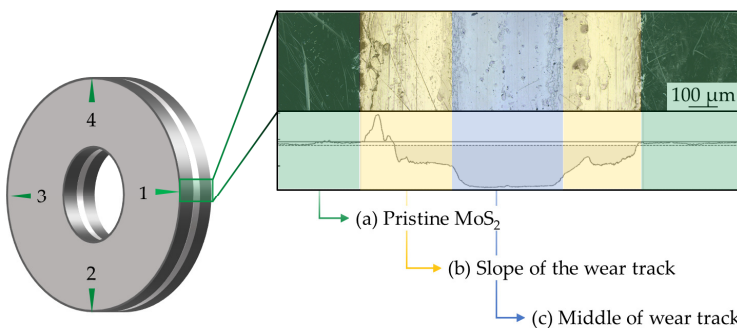


**Figure 2.** Evaluation of the pristine surface and the wear track on the coated discs using LSM and nanoindentation in the designated areas: (a) pristine coating; (b) transition region with compaction of the coating; and (c) worn coating.

As illustrated in Figure 2, the average profile of 50 cross-section measurements was obtained at four points on each specimen, offset by  $90^\circ$  to each other. From the resulting surface profiles, the wear track width and depth were measured, and the wear track area with the arithmetic mean values were calculated. Based on the mean wear area and the circumference, the wear coefficient ( $w_{\text{wear}}$ ) was calculated by corresponding the wear volume ( $W_V$ ) to normal force ( $F_N$ ) and rolling distance ( $s$ ), according to Archard [51].

$$w_{\text{wear}} = \frac{W_V}{F_N \cdot s} \quad (1)$$

### 3. Results and Discussion

#### 3.1. As-Deposited Coating Characterization

The as-deposited coating properties had to be determined first in order to evaluate the changes caused to the coatings due to tribological loading. The results of the LSM measurements and the nanoindentation tests are listed in Table 3. Both coatings showed smooth surfaces with a similar roughness value ( $R_a$ ), indicating that the applied modification with nitrogen caused no significant effect on the roughness. Apart from that, the roughness values are within the known range for sputter-deposited  $\text{MoS}_2$  coatings produced under similar conditions [6,52].

**Table 3.** As-deposited coating properties measured by LSM, EDS, and nanoindentation.

Coating Properties	$\text{MoS}_2$	$\text{MoS}_2:\text{N}$
Roughness $R_a$ in nm	$45 \pm 7$	$46 \pm 7$
Coating thickness in $\mu\text{m}$	$4.0 \pm 0.2$	$2.7 \pm 0.1$
Indentation modulus $E_{\text{IT}}$ in GPa	$7.44 \pm 1.29$	$17.29 \pm 1.40$
Indentation hardness $H_{\text{IT}}$ in GPa	$0.07 \pm 0.02$	$0.56 \pm 0.06$
$\text{O}_2$ content in at %	$3.34 \pm 0.85$	$4.87 \pm 1.21$
S content in at %	$60.57 \pm 0.67$	$55.42 \pm 2.19$
Mo content in at %	$33.13 \pm 0.45$	$30.09 \pm 1.48$
S/Mo-ratio	$1.83 \pm 0.01$	$1.84 \pm 0.03$

Measuring the coating thickness, the difference between the pure and the nitrogen-modified  $\text{MoS}_2$  coating was obvious, and it was noticeable that the modification corresponds to a 32.5% reduced coating thickness for an almost identical deposition time. On the one hand, it is known from previous work [21,22] that pure  $\text{MoS}_2$  coatings deposited by PVD under threefold substrate rotation tend to a certain degree of porosity; therefore, its presence was assumed here as well. On the other hand, the lower coating thickness of  $\text{MoS}_2:\text{N}$  indicated a densification of the coating with fewer pores. For instance, Fu et al. [38] and Hudec et al. [37] demonstrated via scanning electron microscopy and transmission electron microscopy the reduction of pores and, thus, a densification of the  $\text{MoS}_2$ -based coating by adding nitrogen. Another possible explanation was provided by

Hebbar Kannur et al. [40]. In their study, the nitrogen modification resulted in a lower deposition rate due to a mixed nitrogen–argon plasma during the deposition process, thus possibly reducing S and Mo sputtering yields. In our study, the indentation hardness ( $H_{IT}$ ) and indentation modulus ( $E_{IT}$ ) of pure  $\text{MoS}_2$  and  $\text{MoS}_2:\text{N}$  differed significantly for the as-deposited state. Hence, adding nitrogen during the deposition process caused a remarkable upsurge of 700% in  $H_{IT}$  and 132% in  $E_{IT}$  compared to the pure  $\text{MoS}_2$  coating (see Table 3). In turn, these observations indicated the previously suggested densification of the  $\text{MoS}_2:\text{N}$  coating due to nitrogen modification. An enhancement of the mechanical properties by adding nitrogen with similar trends was reported in [37–41].

The chemical composition, measured via EDS, of the coatings showed a sulfur-deficient character and, therefore, a sub-stoichiometric S/Mo-ratio of approximately 1.8. It is known from the literature that resputtering effects can cause a sulfur deficit in  $\text{MoS}_2$  coatings produced by PVD processes [53,54]. In addition, the coatings contained 3–4 at % oxygen, which is attributable to the oxidation of the coatings after the tribological tests during optical characterization in the LSM under atmosphere. Therefore, it was expected that the measured oxygen content did not have any influence on the tribological tests.

### 3.2. Frictional Behavior

Two-disc tests (see Section 2.3) were carried out for a subsequent evaluation of the frictional behavior. The COF curves over cycles for the two performed runs (V1 and V2) of each coating are depicted in Figure 3. While a distinct running-in behavior was observed in all tests during the first 200 cycles, the overall COF is visibly higher for  $\text{MoS}_2$  (Figure 3a) compared to  $\text{MoS}_2:\text{N}$  (Figure 3b).

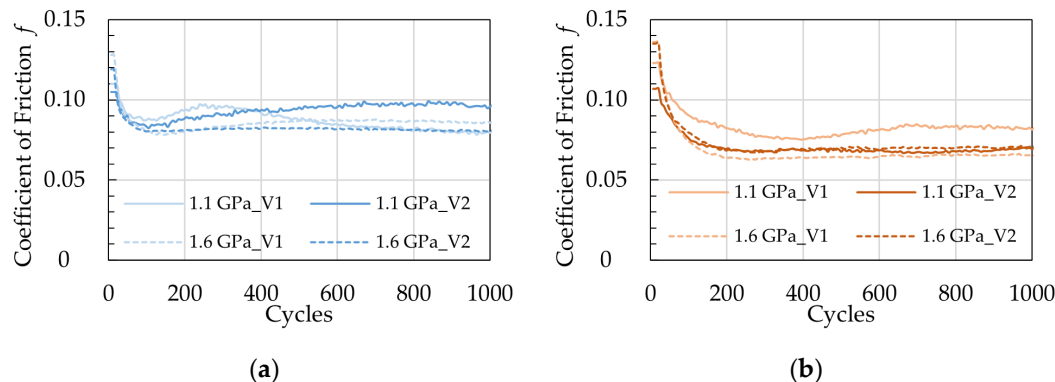


**Figure 3.** COF over the complete testing time (1000 cycles): (a)  $\text{MoS}_2$  and (b)  $\text{MoS}_2:\text{N}$ , for two load cases (solid line 1.1 GPa, and dashed line 1.6 GPa). V1 and V2 represent the two test runs.

The results for the COF are summarized in Table 4. In order to provide comparable values independent of the running-in behavior for each coating, the arithmetic mean over the last 500 cycles—assuming a steady state in the frictional behavior—was calculated. The results revealed that the COF of  $\text{MoS}_2:\text{N}$  decreased by approximately 17% compared to pure  $\text{MoS}_2$  for a Hertzian pressure of 1.1 GPa, and even 20% for 1.6 GPa, respectively. For both  $\text{MoS}_2$ -based coatings, the COF declined slightly with increasing loading. Comparable behavior was observed for the sliding contact in ball-on-disc tests [16,37,39]. It is noteworthy that the steady-state COF for the sliding contact was usually lower than 0.05, so our determined values for the rolling contact were rather high.

**Table 4.** COF as arithmetic mean over the last 500 cycles.

Frictional Behavior	$\text{MoS}_2$		$\text{MoS}_2:\text{N}$	
	1.1 GPa	1.6 GPa	1.1 GPa	1.6 GPa
Mean COF $f_{500-1000}$	$0.090 \pm 0.007$	$0.084 \pm 0.003$	$0.075 \pm 0.007$	$0.068 \pm 0.003$

### 3.3. Coating Compaction

The tribomechanical response of the coatings, represented by  $E_{IT}$  and  $H_{IT}$ , was studied by comparing these parameters before and after tribological loading in the two-disc tests. Figure 4 depicts the results of the measurements for the as-deposited condition and inside the wear track for both coatings. With regard to the results from the wear tracks, eight indentations were considered for evaluation. For the as-deposited  $\text{MoS}_2$  coating, the  $E_{IT}$  and  $H_{IT}$  values were comparable to similar coatings, as previously published [21,22], and, therefore, well in line with expected mechanical properties. These coatings are representative of porous coatings and, in terms of mechanical properties in the as-deposited state, not comparable to dense coatings, deposited under laboratory conditions, which are predominantly reported in the literature [55,56].

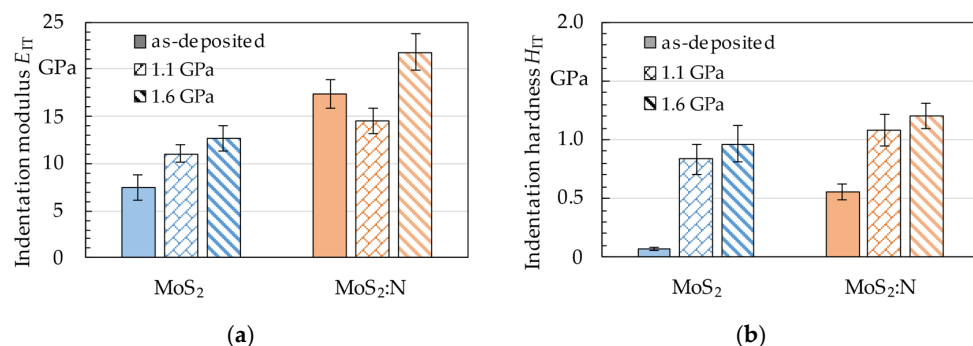


**Figure 4.** Arithmetic mean values for (a) indentation modulus ( $E_{IT}$ ) and (b) indentation hardness ( $H_{IT}$ ) of the respective coatings before (as-deposited) and after tribological loading for two load cases.

As well, the as-deposited MoS<sub>2</sub>:N exhibited increased  $E_{IT}$  (+132%) and  $H_{IT}$  (+700%) values compared to the pure MoS<sub>2</sub> coating, presumably due to its nitrogen-induced increased density, similar to the relative change in hardness observed in other studies [38,39]. After the tribological testing, both coatings showed strongly increased  $E_{IT}$  and  $H_{IT}$  values, which scaled accordingly to the respective load case. For load case 1 (1.1 GPa), pure MoS<sub>2</sub> showed an increase of 48% in  $E_{IT}$  and 1158% in  $H_{IT}$ . For load case 2 (1.6 GPa), an increase of 70% was measured for  $E_{IT}$  and 1337% for  $H_{IT}$ . MoS<sub>2</sub>:N showed, for  $H_{IT}$ , an increase of 96% in load case 1 and 118% in load case 2. The only exception to this tendency occurred for the  $E_{IT}$  value of the MoS<sub>2</sub>:N coating in load case 1, where a decrease of 17% was measured, while, for load case 2, an increase (+25%) was determined, as expected. Fluctuations in the values of the indentation modulus ( $E_{IT}$ ) may be due to small inhomogeneities in the compacted tribofilm, because the  $H_{IT}$  values for the same specimens followed the general trend of increased mechanical properties. Therefore, the improvement of elasticity and hardness for both coatings after tribological testing was attributed to a compaction of the respective coating. Thus, the increased indentation hardness of the MoS<sub>2</sub>:N coating could be correlated with the reduction of the steady-state COF (see Figure 3) in comparison to the pure MoS<sub>2</sub> coating. Similar correlations between hardness and COF were discussed in [57]. Notably,  $H_{IT}$  reached a similar level, regardless of the initial state (as-deposited), and was only slightly dependent on the load. A possible explanation suggested that compaction resulted in an increased density for both coatings according to the applied load. While the as-deposited MoS<sub>2</sub> possessed a more porous, less dense structure [21,22], a higher relative compaction can be achieved compared to the less porous, denser nitrogen-modified MoS<sub>2</sub>:N, exhibiting a lower compaction and, therefore, a reduced relative increase of  $E_{IT}$  and  $H_{IT}$ . The remaining difference in elasticity and hardness might be attributable to the modification with nitrogen.

### 3.4. Wear Behavior

The resulting wear was acquired and quantified according to Section 2.3. Representative LSM images of specimen couples (coated basebody and uncoated counterpart) are

provided in Figure 5 for each coating–load combination. Similar wear tracks were observed for each coating and its counterpart for both load cases. The width and appearance of the pronounced wear track were described qualitatively in Section 2.3, except that MoS<sub>2</sub>:N appeared to have residual coating on the slopes of the wear track.

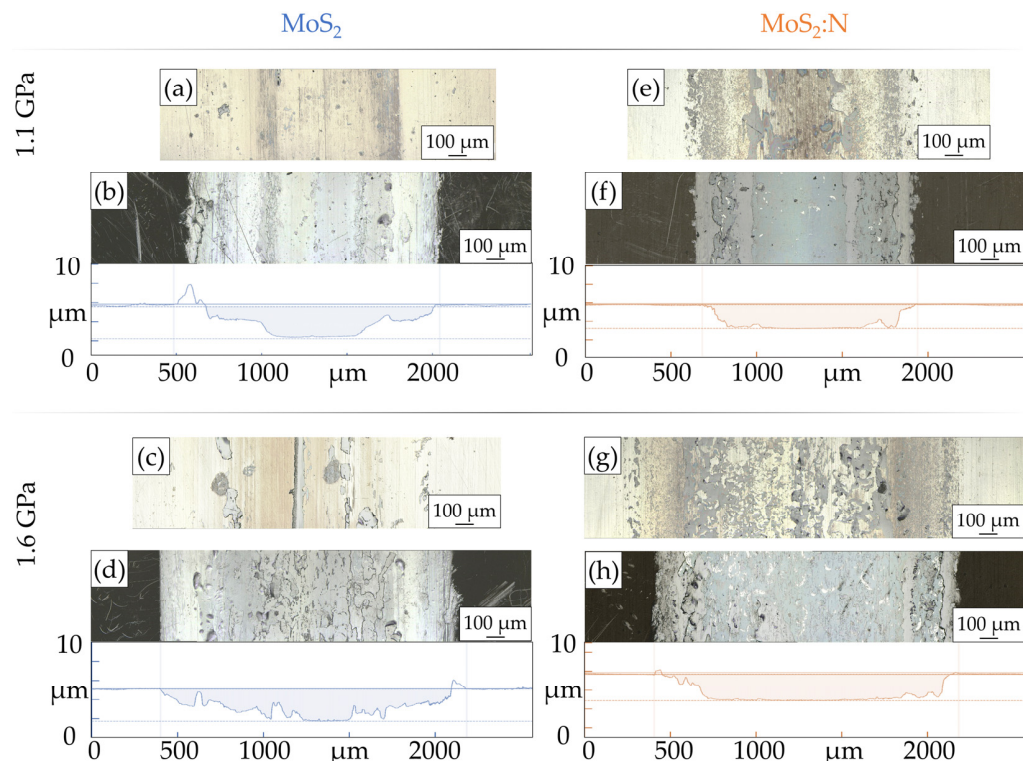


**Figure 5.** (a,c,e,g) Overview of the surfaces of the counterpart and (b,d,f,h) basebody for both coatings after testing in two load cases at 1.1 GPa and 1.6 GPa. Representative images acquired by LSM measurements.

The visible darker residual spots on the counterparts (Figure 5a,c,e,g) indicate a partial coating transfer, as shown in previous studies in which an investigation of coating transfer with energy dispersive spectroscopy or transmission electron microscopy was observed [6,41,58]. The matching pattern of the basebody and counterpart for each coating and load case, therefore, represent that coating transfer occurred (see Figures 6 and 7) and will henceforth be referred to as such.

To obtain a more detailed analysis of the aforementioned coating transfer on the counterpart after the tribological tests, EDS measurements were carried out on the counterparts' surface. Mapping results over the width of the wear tracks are shown for MoS<sub>2</sub> in Figure 6 and for MoS<sub>2</sub>:N in Figure 7. In the case of the MoS<sub>2</sub> coating, the mappings revealed almost no coating transfer for load case 1 (1.1 GPa), as evidenced by a high concentration of Fe in the element mapping due to a large number of purple dots (Figure 6b), which is indicative of the steel substrate. Mo and S showed no distinct measurement signals except for one MoS<sub>2</sub> wear debris (Figure 6c,d). At higher pressure in load case 2, however, more coating transfer was observed, especially in the center of the wear track and the slope areas (Figure 6g,h).

As already indicated by the images of the optical analysis in the LSM, even more coating was transferred to the counterpart in the case of the nitrogen-modified coatings (MoS<sub>2</sub>:N). Figure 7b showed some faint purple areas for load case 1 for the Fe concentration in the element mapping, which, in turn, matched the mappings of Mo (Figure 7c) and S (Figure 7d). Thus, this is clear evidence of partial transfer coating formation. In load case 2 with higher pressure, a pronounced coating transfer was observed, extending almost over the entire width of the wear track, but varying in its concentration (see Figure 7g,h). For both

load cases and coatings, no indication of oxygen was visible in the measurements. In terms of the coating transfer, a certain amount of partial coating transfer occurred, depending on the load case and coating, which, in turn, contributes to the self-lubricating mechanism.

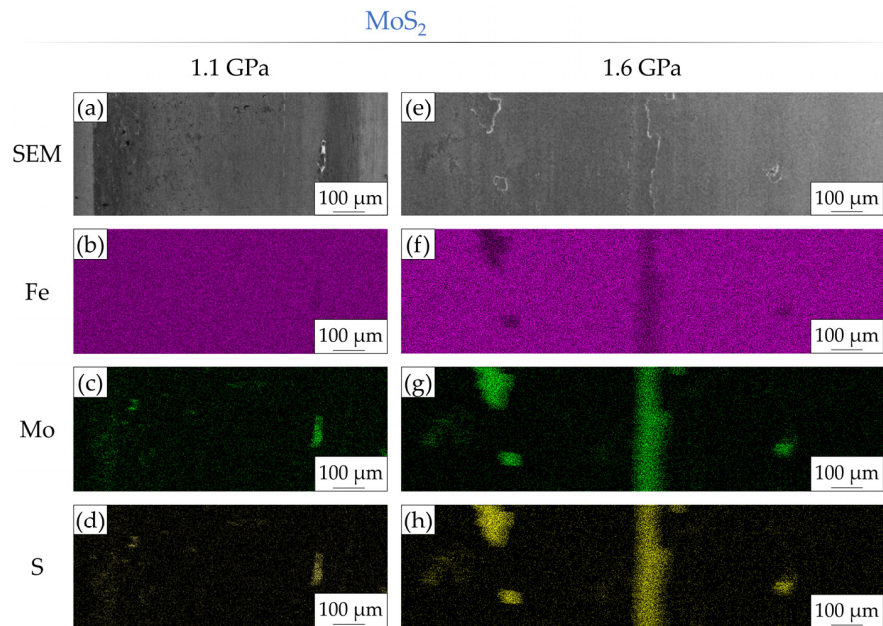


**Figure 6.** SEM images and EDS element mappings for the  $\text{MoS}_2$  counterpart of the load cases 1.1 GPa, (a–d) and 1.6 GPa, (e–h).

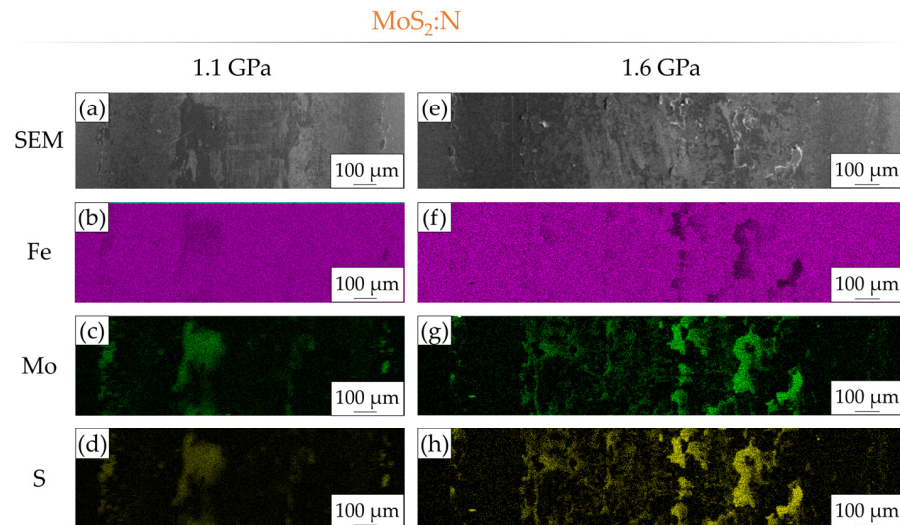


**Figure 7.** SEM images and EDS element mappings for the  $\text{MoS}_2:\text{N}$  counterpart of the load cases 1.1 GPa, (a–d) and 1.6 GPa, (e–h).

Besides the optical matching of the wear tracks, the measured width of the resulting profile and depth of the wear track were also analyzed. The calculated arithmetic mean values are listed in Table 5.

With higher loads, the wear coefficient  $w_{\text{wear}}$  was similar for both coatings with a value of about  $4 \times 10^{-6} \text{ mm}^3 \text{ N}^{-1} \text{ m}^{-1}$ . A negligible change in depth  $h_{\text{wear}}$  and a clear increase in width  $b_{\text{wear}}$  was determined for both coatings after applying load case 2. As a result, the wear area  $A_{\text{wear}}$  depended mainly on the change of the wear track width. For  $\text{MoS}_2$ , only a slight increase in width  $b_{\text{wear}}$  was measured after applying 1.6 GPa and the resulting wear area was only increased by 7%. This divergence can be considered to be within the accumulated fluctuations for materials, coatings, and testing-rig, and, in fact,

would suggest that the tribological behavior of  $\text{MoS}_2$  can be assumed to be the same for both load cases.

**Table 5.** Mean values of the wear track on the coated specimens and calculated wear coefficient according to Archard [51].

Wear Behavior	$\text{MoS}_2$		$\text{MoS}_2:\text{N}$	
	1.1 GPa	1.6 GPa	1.1 GPa	1.6 GPa
Mean wear track depth $h_{\text{wear}}$ in $\mu\text{m}$	3.19 $\pm 0.27$	3.02 $\pm 0.40$	2.65 $\pm 0.14$	2.62 $\pm 0.14$
Mean wear track width $b_{\text{wear}}$ in mm	1.54 $\pm 0.06$	1.79 $\pm 0.06$	1.34 $\pm 0.02$	1.88 $\pm 0.04$
Mean wear track area $A_{\text{wear}}$ in $\text{mm}^2$	2.54 $\pm 0.25$	2.73 $\pm 0.44$	2.16 $\pm 0.41$	3.24 $\pm 0.29$
Mean wear coefficient $w_{\text{wear}}$ in $10^{-6} \times \text{mm}^3 \text{N}^{-1} \text{m}^{-1}$	9.57 $\pm 0.96$	4.05 $\pm 0.65$	8.14 $\pm 1.56$	4.79 $\pm 0.42$

As depicted in Figure 5a–d, for all  $\text{MoS}_2$  tests, primarily the middle of the wear track showed (little) signs of coating transfer, indicated by the matching pattern on the counterpart. The same behavior was observed for  $\text{MoS}_2:\text{N}$  (Figure 5e–h), with the difference of the wear track slopes of the basebody, displaying the accumulated coating alongside the movement direction (Figure 5f,h). A more detailed illustration of the transition from the middle of the wear track to the slope of the wear track is depicted in Figure 8. From these images, it was demonstrated that a steady transition for  $\text{MoS}_2$  could be found from the wear track to the slope and to the pristine  $\text{MoS}_2$ . The middle of the wear track was identified as compacted  $\text{MoS}_2$  by means of wear track depth  $h_{\text{wear}}$ —which is lower than the initial coating thickness—and the measured indentation hardness  $H_{\text{IT}}$ , which were similar to values measured for the  $\text{MoS}_2$  coating, which was verified to be compacted [21,22]. Insofar as the coatings were already prepared dense in the as-deposited state, such phenomena were not monitored.

In addition, the pattern of the residual coating suggested that, in case of  $\text{MoS}_2$ , the homogenous coating remained in the middle of the wear track, while the slopes of the wear track appeared to be mostly composed of the compacted coating originating from the contact area. In contrast, for  $\text{MoS}_2:\text{N}$ , the apparent residual coating on the slope of the wear track and the mean wear track depth  $h_{\text{wear}}$ , matching the coating thickness, suggested a different wear mechanism during testing.

Based on the optical analysis of the wear tracks, it was assumed that the difference in the wear mechanisms, schematically depicted in Figure 9, was dependent on the coating, specifically the thickness. While the initial contact seemed to be independent of the load case for each coating, the resulting wear tracks were different. Thus, during testing (Figure 9b), it was assumed, for both coatings, that wear and subsequent coating transfer, the typical lubrication mechanism for dry lubrication [59,60], occurred. The provided coating thickness was sufficient; compaction could occur in this area, in addition to coating transfer. The occurring wear debris, which was neither transferred nor compacted, was expected to be pressed along the slopes of the wear track (Figure 9c). As the transferred coating of pure  $\text{MoS}_2$  was found just in the middle of the wear track, it was considered that dry lubrication occurred mainly in the middle of the wear track on the compacted coating. In comparison, for  $\text{MoS}_2:\text{N}$ , the residual coating was found on both the basebody and its counterpart (see Figure 7) in the middle and the slopes of the wear track. While it seemed apparent that the worn coating in the middle was mainly transferred to the counterpart (evidence in Figure 7), it was also assumed that the accumulated coating on the slopes of the wear track served as the ‘rails’ for the counterpart. This thesis was supported by the matching residual coating visible on the specimens and the slightly lower COF, despite the worn coating. In conclusion, it was found that, on the one hand, under sliding–rolling conditions, a compaction of the  $\text{MoS}_2$  coating occurred and provided a functional surface for dry lubrication, while, on the other hand, this compaction was dependent on the coating thickness and could lead to a different wear mechanism (see Figure 9).

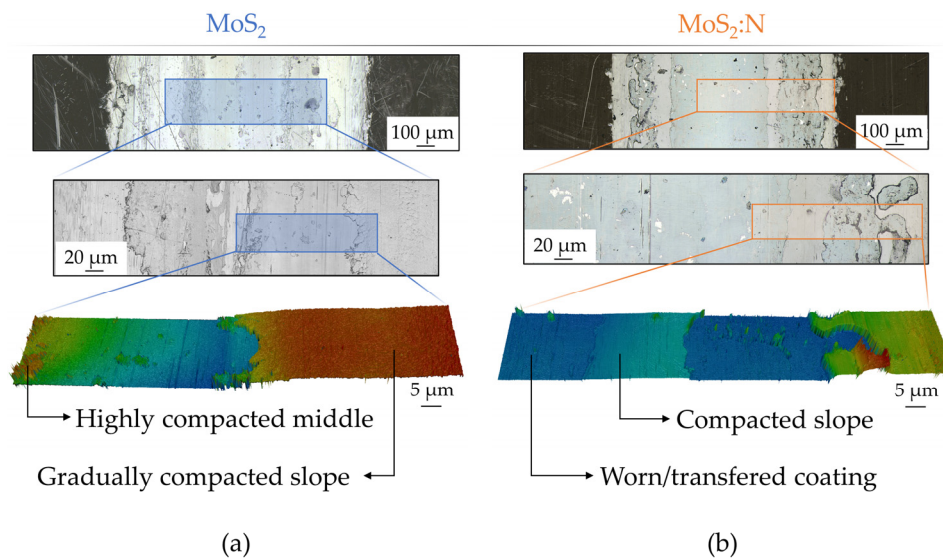


**Figure 8.** Surface of the wear tracks of both coatings at increased magnification: (a) a continuous slope was observed for  $\text{MoS}_2$  and (b) a partially worn slope of the wear track for  $\text{MoS}_2:\text{N}$ .

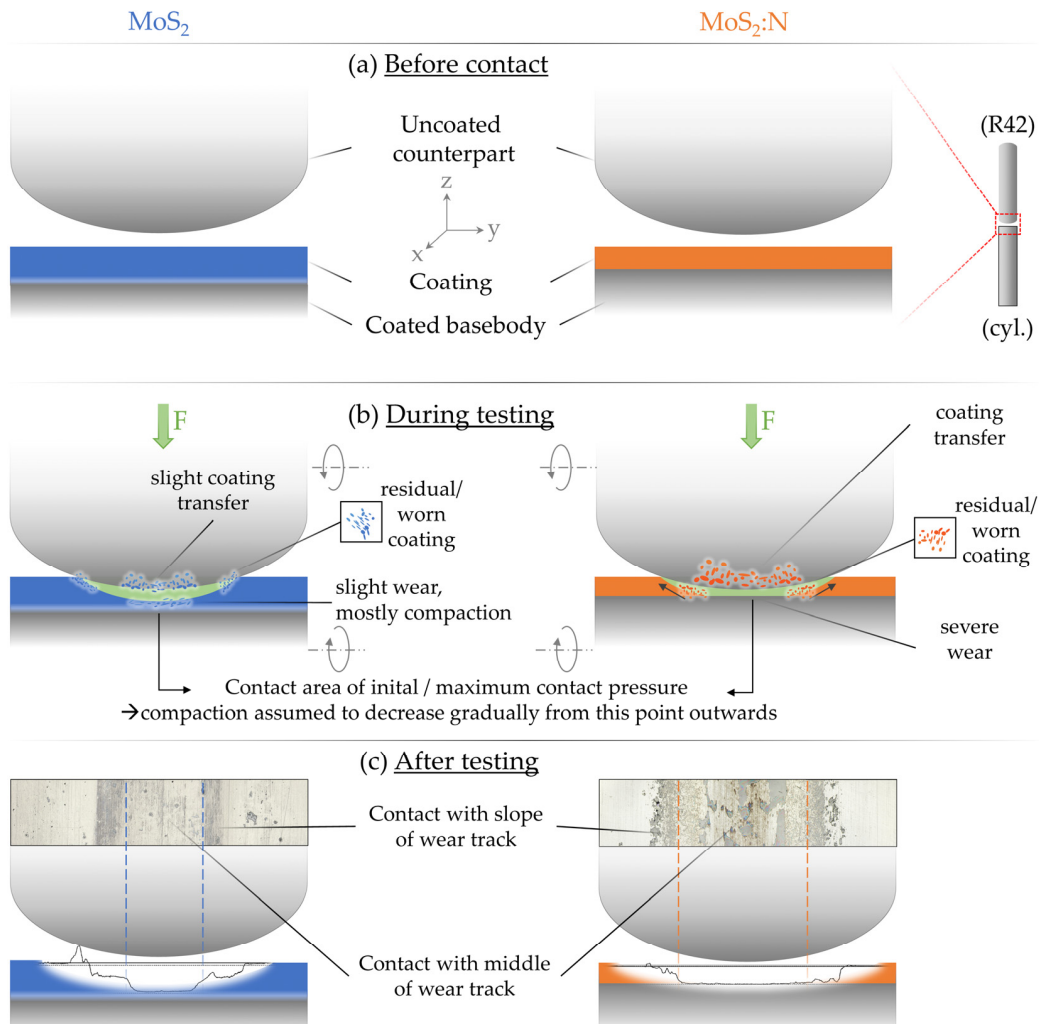


**Figure 9.** Schematic depiction of the assumed stages of the tribological testing and the resulting wear mechanisms: (a) initial set-up before contact, (b) during the tribological testing, and (c) resulting wear track and coating transfer after tribological tests.

#### 4. Conclusions

This work presented the behavior of nitrogen-modified PVD–MoS<sub>2</sub> coatings in terms of tribological behavior under rolling–sliding conditions in a vacuum, tested on a 2DT.

Regarding the mechanical properties of the as-deposited coatings, an increase in the indentation modulus of 132% and indentation hardness of 700% due to adding nitrogen could be noticed, which was attributed to an assumed densification of the microstructure, as indicated by a relative comparison of coating thickness and as reported in literature before [37,38]. Moreover, the nitrogen modification resulted in a 17% reduction of the COF in the two-disc tests. The COF was reduced with increasing pressure for both coating variants (MoS<sub>2</sub> 6.6% and MoS<sub>2</sub>:N 9.3%). The tribologically induced compaction of the initially porous coatings was verified after testing, on the one hand, by an increase in the indentation hardness of the formed tribofilm in the wear tracks (for MoS<sub>2</sub> 1158% and 1337% for load case 1 and 2, respectively, and for MoS<sub>2</sub>:N 96% and 118%) and, on the other hand, on profiling in the cross-section of the wear tracks.

Based on the results, two wear mechanisms can be concluded: the pure MoS<sub>2</sub> coatings were mainly compacted in the center of the contact area and the dry-lubrication effect was maintained without noticeable transfer to the counterpart. Under tribological loading, the MoS<sub>2</sub>:N coating was pressed to the slope of the wear track and compacted there, with the additional transfer of the tribofilm to the counterpart occurring predominantly in the contact center but, also, on the slopes of the wear track. Both together caused a successful lubrication effect. However, these wear mechanisms were not load-dependent, but coating-dependent. This was also shown in the evaluation of the wear phenomena on the coated basebody, because the wear depth was almost identical, although the wear track width became wider due to higher loads and, thus, resulted in a larger wear area.

**Author Contributions:** Conceptualization, A.S. and M.P.; data curation, A.S. and M.P.; formal analysis, A.S. and M.P.; funding acquisition, S.T.; investigation, A.S.; methodology, A.S. and S.T.; resources, S.W.; supervision, M.B., S.T. and S.W.; visualization, A.S. and M.P.; writing—original draft preparation, A.S. and M.P.; writing—review and editing, M.B., S.W. and S.T. All authors have read and agreed to the published version of the manuscript.

**Funding:** This research was funded by the German Research Foundation, grant number (GEPRIS) 407707942.

**Data Availability Statement:** All data needed to evaluate the conclusions are present in the paper. Additional data may be requested from the authors.

**Acknowledgments:** The authors thank M. Göken and M. Köbrich (Materials Science and Engineering I, Friedrich-Alexander-Universität Erlangen-Nürnberg (FAU)) for providing access to the laboratory equipment and the performance of the SEM-EDS measurements. The authors greatly acknowledge the continuous support of Universität Bayreuth and Friedrich-Alexander-Universität Erlangen-Nürnberg (FAU).

**Conflicts of Interest:** The authors declare no conflict of interest.

#### References

1. Vazirisereshk, M.R.; Martini, A.; Strubbe, D.A.; Baykara, M.Z. Solid Lubrication with MoS<sub>2</sub>: A Review. *Lubricants* **2019**, *7*, 57. [[CrossRef](#)]
2. Marian, M.; Berman, D.; Rota, A.; Jackson, R.L.; Rosenkranz, A. Layered 2D Nanomaterials to Tailor Friction and Wear in Machine Elements—A Review. *Adv Mater. Inter* **2022**, *9*, 2101622. [[CrossRef](#)]
3. Gradt, T.; Schneider, T. Tribological Performance of MoS<sub>2</sub> Coatings in Various Environments. *Lubricants* **2016**, *4*, 32. [[CrossRef](#)]
4. Koch, F.; Nocentini, R.; Heinemann, B.; Lindig, S.; Junghanns, P.; Bolt, H. MoS<sub>2</sub> coatings for the narrow support elements of the W-7X nonplanar coils. *Fusion Eng. Des.* **2007**, *82*, 1614–1620. [[CrossRef](#)]
5. Serles, P.; Gaber, K.; Pajovic, S.; Colas, G.; Filteeter, T. High Temperature Microtribological Studies of MoS<sub>2</sub> Lubrication for Low Earth Orbit. *Lubricants* **2020**, *8*, 49. [[CrossRef](#)]
6. Prozhega, M.V.; Kharkov, M.M.; Reschikov, E.O.; Rykunov, G.I.; Kaziev, A.V.; Kukushkina, M.S.; Kolodko, D.V.; Stepanova, T.V. Estimation of MoS<sub>2</sub> Coating Performance on Bronze and Steel in Vacuum at High Temperatures. *Coatings* **2022**, *12*, 125. [[CrossRef](#)]
7. Roberts, E.W. Space tribology: Its role in spacecraft mechanisms. *J. Phys. D Appl. Phys.* **2012**, *45*, 503001. [[CrossRef](#)]

8. Donnet, C.; Martin, J.M.; Le Mogne, T.; Belin, M. Super-low friction of MoS<sub>2</sub> coatings in various environments. *Tribol. Int.* **1996**, *29*, 123–128. [[CrossRef](#)]
9. Mukhtar, S.H.; Wani, M.F.; Sehgal, R.; Sharma, M.D. Nano-mechanical and nano-tribological characterisation of self-lubricating MoS<sub>2</sub> nano-structured coating for space applications. *Tribol. Int.* **2023**, *178*, 108017. [[CrossRef](#)]
10. Babuska, T.F.; Curry, J.F.; Dugger, M.T.; Lu, P.; Xin, Y.; Klueter, S.; Kozen, A.C.; Grejtak, T.; Krick, B.A. Role of Environment on the Shear-Induced Structural Evolution of MoS<sub>2</sub> and Impact on Oxidation and Tribological Properties for Space Applications. *ACS Appl. Mater. Interfaces* **2022**, *14*, 13914–13924. [[CrossRef](#)]
11. Hilton, M.R.; Fleischauer, P.D. TEM lattice imaging of the nanostructure of early-growth sputter-deposited MoS<sub>2</sub> solid lubricant films. *J. Mater. Res.* **1990**, *5*, 406–421. [[CrossRef](#)]
12. Pan, S.; Jin, K.; Wang, T.; Zhang, Z.; Zheng, L.; Umebara, N. Metal matrix nanocomposites in tribology: Manufacturing, performance, and mechanisms. *Friction* **2022**, *10*, 1596–1634. [[CrossRef](#)]
13. Furlan, K.P.; de Mello, J.D.B.; Klein, A.N. Self-lubricating composites containing MoS<sub>2</sub>: A review. *Tribol. Int.* **2018**, *120*, 280–298. [[CrossRef](#)]
14. Donnet, C.; Le Mogne, T.; Martin, J.M. Superlow friction of oxygen-free MoS<sub>2</sub> coatings in ultrahigh vacuum. *Surf. Coat. Technol.* **1993**, *62*, 406–411. [[CrossRef](#)]
15. Le Mogne, T.; Donnet, C.; Martin, J.M.; Tonck, A.; Millard-Pinard, N.; Fayeulle, S.; Moncoffre, N. Nature of super-lubricating MoS<sub>2</sub> physical vapor deposition coatings. *J. Vac. Sci. Technol. A Vac. Surf. Film.* **1994**, *12*, 1998–2004. [[CrossRef](#)]
16. Zhang, Y.; Li, P.; Ji, L.; Liu, X.; Wan, H.; Chen, L.; Li, H.; Jin, Z. Tribological properties of MoS<sub>2</sub> coating for ultra-long wear-life and low coefficient of friction combined with additive g-C3N4 in air. *Friction* **2021**, *9*, 789–801. [[CrossRef](#)]
17. Domínguez-Meister, S.; Rojas, T.C.; Brizuela, M.; Sánchez-López, J.C. Solid lubricant behavior of MoS<sub>2</sub> and WSe<sub>2</sub>-based nanocomposite coatings. *Sci. Technol. Adv. Mater.* **2017**, *18*, 122–133. [[CrossRef](#)]
18. Zhang, X.; Lauwerens, W.; He, J.; Celis, J.-P. Structure and growth of basal and random oriented MoS<sub>x</sub> coatings deposited by magnetron sputtering. *J. Vac. Sci. Technol. A Vac. Surf. Film.* **2003**, *21*, 416–421. [[CrossRef](#)]
19. Vierneusel, B.; Schneider, T.; Tremmel, S.; Wartzack, S.; Gradt, T. Humidity resistant MoS<sub>2</sub> coatings deposited by unbalanced magnetron sputtering. *Surf. Coat. Technol.* **2013**, *235*, 97–107. [[CrossRef](#)]
20. Muratore, C.; Voevodin, A.A. Control of molybdenum disulfide basal plane orientation during coating growth in pulsed magnetron sputtering discharges. *Thin Solid Film.* **2009**, *517*, 5605–5610. [[CrossRef](#)]
21. Krauß, S.; SeyNSTAHL, A.; Tremmel, S.; Meyer, B.; Bitzek, E.; Göken, M.; Yokosawa, T.; Zubiri, B.A.; Spiecker, E.; Merle, B. Structural reorientation and compaction of porous MoS<sub>2</sub> coatings during wear testing. *Wear* **2022**, *500–501*, 204339. [[CrossRef](#)]
22. SeyNSTAHL, A.; Krauß, S.; Bitzek, E.; Meyer, B.; Merle, B.; Tremmel, S. Microstructure, Mechanical Properties and Tribological Behavior of Magnetron-Sputtered MoS<sub>2</sub> Solid Lubricant Coatings Deposited under Industrial Conditions. *Coatings* **2021**, *11*, 455. [[CrossRef](#)]
23. Bondarev, A.; Ponomarev, I.; Muydinov, R.; Polcar, T. Friend or Foe? Revising the Role of Oxygen in the Tribological Performance of Solid Lubricant MoS<sub>2</sub>. *ACS Appl. Mater. Interfaces* **2022**, *14*, 55051–55061. [[CrossRef](#)]
24. Wang, J.; Lauwerens, W.; Weiers, E.; Stals, L.M.; He, J.; Celis, J.P. Structure and tribological properties of MoS<sub>x</sub> coatings prepared by bipolar DC magnetron sputtering. *Surf. Coat. Technol.* **2001**, *139*, 143–152. [[CrossRef](#)]
25. Babuska, T.F.; Curry, J.F.; Thorpe, R.; Chowdhury, M.I.; Strandwitz, N.C.; Krick, B.A. High-Sensitivity Low-Energy Ion Spectroscopy with Sub-Nanometer Depth Resolution Reveals Oxidation Resistance of MoS<sub>2</sub> Increases with Film Density and Shear-Induced Nanostructural Modifications of the Surface. *ACS Appl. Nano Mater.* **2023**, *6*, 1153–1160. [[CrossRef](#)] [[PubMed](#)]
26. Serles, P.; Sun, H.; Colas, G.; Tam, J.; Nicholson, E.; Wang, G.; Howe, J.; Saulot, A.; Singh, C.V.; Filteer, T. Structure-Dependent Wear and Shear Mechanics of Nanostructured MoS<sub>2</sub> Coatings. *Adv. Mater. Inter.* **2020**, *7*, 1901870. [[CrossRef](#)]
27. Ding, X.; Zeng, X.T.; He, X.Y.; Chen, Z. Tribological properties of Cr- and Ti-doped MoS<sub>2</sub> composite coatings under different humidity atmosphere. *Surf. Coat. Technol.* **2010**, *205*, 224–231. [[CrossRef](#)]
28. Lu, X.; Yan, M.; Yan, Z.; Chen, W.; Sui, X.; Hao, J.; Liu, W. Exploring the atmospheric tribological properties of MoS<sub>2</sub>-(Cr, Nb, Ti, Al, V) composite coatings by high throughput preparation method. *Tribol. Int.* **2021**, *156*, 106844. [[CrossRef](#)]
29. Wang, X.; Xing, Y.; Ma, S.; Zhang, X.; Xu, K.; Teer, D.G. Microstructure and mechanical properties of MoS<sub>2</sub>/titanium composite coatings with different titanium content. *Surf. Coat. Technol.* **2007**, *201*, 5290–5293. [[CrossRef](#)]
30. Stoyanov, P.; Fishman, J.Z.; Lince, J.R.; Chromik, R.R. Micro-tribological performance of MoS<sub>2</sub> lubricants with varying Au content. *Surf. Coat. Technol.* **2008**, *203*, 761–765. [[CrossRef](#)]
31. Chien, H.-H.; Ma, K.-J.; Vattikuti, S.P.; Kuo, C.-H.; Huo, C.-B.; Chao, C.-L. Tribological behaviour of MoS<sub>2</sub>/Au coatings. *Thin Solid Film.* **2010**, *518*, 7532–7534. [[CrossRef](#)]
32. Yin, X.; Jin, J.; Chen, X.; Ma, T.; Zhang, C. A New Pathway for Superlubricity in a Multilayered MoS<sub>2</sub>-Ag Film under Cryogenic Environment. *Nano Lett.* **2021**, *21*, 10165–10171. [[CrossRef](#)] [[PubMed](#)]
33. Zhao, X.; Lu, Z.; Wu, G.; Zhang, G.; Wang, L.; Xue, Q. Preparation and properties of DLC/MoS<sub>2</sub> multilayer coatings for high humidity tribology. *Mater. Res. Express* **2016**, *3*, 66401. [[CrossRef](#)]
34. Niakan, H.; Zhang, C.; Hu, Y.; Szpunar, J.A.; Yang, Q. Thermal stability of diamond-like carbon–MoS<sub>2</sub> thin films in different environments. *Thin Solid Film.* **2014**, *562*, 244–249. [[CrossRef](#)]

35. Baker, C.C.; Voevodin, A.A.; Zabinski, J.S. Comparison of WC/DLC/WS<sub>2</sub> and YSZ/Au/DLC/MoS<sub>2</sub> “Chameleon” Coatings for Tribological Applications. In *World Tribology Congress III, Volume 2*; World Tribology Congress III: Washington, DC, USA, 2005; pp. 379–380. ISBN 0-7918-4202-9.
36. Baker, C.C.; Chromik, R.R.; Wahl, K.J.; Hu, J.J.; Voevodin, A.A. Preparation of chameleon coatings for space and ambient environments. *Thin Solid Film.* **2007**, *515*, 6737–6743. [[CrossRef](#)]
37. Hudec, T.; Roch, T.; Gregor, M.; Orovčík, L.; Mikula, M.; Polcar, T. Tribological behaviour of Mo-S-N solid lubricant coatings in vacuum, nitrogen gas and elevated temperatures. *Surf. Coat. Technol.* **2021**, *405*, 126722. [[CrossRef](#)]
38. Fu, Y.; He, T.; Yang, W.; Xu, J.; Mu, B.; Pang, X.; Wang, P. Structure, Mechanical and Tribological Properties of MoS<sub>N</sub>/MoS<sub>2</sub> Multilayer Films. *Coatings* **2019**, *9*, 108. [[CrossRef](#)]
39. Hebbar Kannur, K.; Yaqub, T.B.; Pupier, C.; Héau, C.; Cavaleiro, A. Mechanical Properties and Vacuum Tribological Performance of Mo-S-N Sputtered Coatings. *ACS Appl. Mater. Interfaces* **2020**, *12*, 43299–43310. [[CrossRef](#)]
40. Hebbar Kannur, K.; Yaqub, T.B.; Huminicu, T.; Polcar, T.; Pupier, C.; Héau, C.; Cavaleiro, A. Synthesis and structural properties of Mo-S-N sputtered coatings. *Appl. Surf. Sci.* **2020**, *527*, 146790. [[CrossRef](#)]
41. Hudec, T.; Mikula, M.; Satrapinskyy, L.; Roch, T.; Truchly, M.; Švec, P.; Huminicu, T.; Polcar, T. Structure, mechanical and tribological properties of Mo-S-N solid lubricant coatings. *Appl. Surf. Sci.* **2019**, *486*, 1–14. [[CrossRef](#)]
42. Patzer, G.; Woydt, M.; Shah, R.; Miller, C.; Iaccarino, P. Test Modes for Establishing the Tribological Profile under Slip-Rolling. *Lubricants* **2020**, *8*, 59. [[CrossRef](#)]
43. Woydt, M.; Scholz, C.; Burbank, J.; Spaltmann, D. Slip-rolling resistant steel alloys up to P0max of 3,920 MPa. *Wear* **2021**, *474*–475, 203707. [[CrossRef](#)]
44. Polzer, M.; Bartz, M.; Rothammer, B.; Schulz, E.; Wartzack, S. Tribological behavior of different doped ta-C coatings for slip-rolling contacts with high hertzian contact pressure. *ILT*, 2023; *ahead-of-print*. [[CrossRef](#)]
45. Burbank, J.; Woydt, M. Friction and wear reductions in slip-rolling steel contacts through pre-conditioned chemical tribofilms from bismuth compounds. *Wear* **2016**, *360*–361, 29–37. [[CrossRef](#)]
46. Yilmaz, M.; Kratzer, D.; Lohner, T.; Michaelis, K.; Stahl, K. A study on highly-loaded contacts under dry lubrication for gear applications. *Tribol. Int.* **2018**, *128*, 410–420. [[CrossRef](#)]
47. Hofmann, S.; Yilmaz, M.; Maier, E.; Lohner, T.; Stahl, K. Friction and contact temperature in dry rolling-sliding contacts with MoS<sub>2</sub>-bonded and a-C:H:Zr DLC coatings. *Int. J. Mech. Mater. Eng.* **2021**, *16*, 9. [[CrossRef](#)]
48. Oliver, W.C.; Pharr, G.M. An improved technique for determining hardness and elastic modulus using load and displacement sensing indentation experiments. *J. Mater. Res.* **1992**, *7*, 1564–1583. [[CrossRef](#)]
49. Oliver, W.C.; Pharr, G.M. Measurement of hardness and elastic modulus by instrumented indentation: Advances in understanding and refinements to methodology. *J. Mater. Res.* **2004**, *19*, 3–20. [[CrossRef](#)]
50. Bückle, H.; Frank, K. *Mikrohärteprüfung und Ihre Anwendung*; Berliner Union: Stuttgart, Germany, 1965.
51. Archard, J.F. Contact and Rubbing of Flat Surfaces. *J. Appl. Phys.* **1953**, *24*, 981–988. [[CrossRef](#)]
52. Dreva, K.; Morina, A.; Yang, L.; Neville, A. The effect of temperature on water desorption and oxide formation in MoS<sub>2</sub> coatings and its impact on tribological properties. *Surf. Coat. Technol.* **2022**, *433*, 128077. [[CrossRef](#)]
53. Rigato, V.; Maggioni, G.; Patelli, A.; Boscarino, D.; Renevier, N.; Teer, D. Properties of sputter-deposited MoS<sub>2</sub>/metal composite coatings deposited by closed field unbalanced magnetron sputter ion plating. *Surf. Coat. Technol.* **2000**, *131*, 206–210. [[CrossRef](#)]
54. Buck, V. Lattice parameters of sputtered MoS<sub>2</sub> films. *Thin Solid Film.* **1991**, *198*, 157–167. [[CrossRef](#)]
55. Renevier, N.; Fox, V.; Teer, D.; Hampshire, J. Coating characteristics and tribological properties of sputter-deposited MoS<sub>2</sub>/metal composite coatings deposited by closed field unbalanced magnetron sputter ion plating. *Surf. Coat. Technol.* **2000**, *127*, 24–37. [[CrossRef](#)]
56. Simmonds, M.; Savan, A.; Pflüger, E.; van Swygenhoven, H. Mechanical and tribological performance of MoS<sub>2</sub> co-sputtered composites. *Surf. Coat. Technol.* **2000**, *126*, 15–24. [[CrossRef](#)]
57. Pan, S.; Saso, T.; Yu, N.; Sokoluk, M.; Yao, G.; Umehara, N.; Li, X. New study on tribological performance of AA7075-TiB<sub>2</sub> nanocomposites. *Tribol. Int.* **2020**, *152*, 106565. [[CrossRef](#)]
58. Sklenak, S.; Brimmers, J.; Brecher, C. Analyse der Wirkmechanismen im fluidfreien Wälzkontakt mit beschichteten Oberflächen. *Fortsch. Ing.* **2022**, *86*, 357–366. [[CrossRef](#)]
59. Yang, Z.; Bhowmick, S.; Sen, F.G.; Alpas, A.T. Microscopic and atomistic mechanisms of sliding friction of MoS<sub>2</sub>: Effects of undissociated and dissociated H<sub>2</sub>O. *Appl. Surf. Sci.* **2021**, *563*, 150270. [[CrossRef](#)]
60. Marian, M.; Feile, K.; Rothammer, B.; Bartz, M.; Wartzack, S.; Seynsthahl, A.; Tremmel, S.; Krauß, S.; Merle, B.; Böhm, T.; et al. Ti<sub>3</sub>C<sub>2</sub>T<sub>x</sub> solid lubricant coatings in rolling bearings with remarkable performance beyond state-of-the-art materials. *Appl. Mater. Today* **2021**, *25*, 101202. [[CrossRef](#)]

**Disclaimer/Publisher’s Note:** The statements, opinions and data contained in all publications are solely those of the individual author(s) and contributor(s) and not of MDPI and/or the editor(s). MDPI and/or the editor(s) disclaim responsibility for any injury to people or property resulting from any ideas, methods, instructions or products referred to in the content.